

The neutron magnetic form factor $G_M^n(Q^2)$ from Quasi-Elastic inclusive scattering data on D and ^4He

A.S. Rinat and M.F. Taragin

Weizmann Institute of Science, Department of Particle Physics, Rehovot 76100, Israel

M. Viviani

INFN, Sezione Pisa and Phys. Dept., University of Pisa, I-56100, Italy

(Dated: May 22, 2019)

We analyze cross sections for Quasi-Elastic inclusive scattering of electrons on nuclei and show that the observed isolated peaks for relatively low Q^2 are unique for the lightest targets. Focusing in particular on D and ^4He , we investigate in two ways to what measure the above peaks can be allocated to nucleon-elastic processes. We first compute approximate upper limits for the nucleon-inelastic background in the Quasi-Elastic region due to inclusive Δ excitation, and find those to be small. Far more precise is a semi-phenomenological approach, where the dominance of nucleon-elastic processes is translated into a set of stringent requirements. We show that those are very well fulfilled for recent D data, and to a somewhat lesser extent for older D and ^4He data. With knowledge of $G_{E,M}^p$ and information on G_E^n , we then extract G_M^n and find agreement with values obtained by alternative methods. We discuss the sensitivity of the extraction method and mention future applications.

I. INTRODUCTION.

Charge-current distributions of hadrons are basic sources of information, which may be compared with predictions of fundamental theories. Examples are static form factors of the neutron and its structure functions (SF) which depend on those distributions. Over many years, experimental efforts have been made to extract those observables with maximal accuracy. This requires high-quality data, and in parallel, accurate control of nuclear medium effects. In this note we focus on the magnetic form factor of the neutron.

A standard tool for the study of $G_M^n(Q^2)$ has been Quasi-Elastic (QE) electron scattering on a D for relatively low Q^2 . We also mention semi-inclusive scattering experiments $D(e, e'N)X$, where $N = p$ or n [1, 2], as well as total inclusive data on D up to $Q^2 \leq 4 \text{ GeV}^2$ [3]. The varied kinematics in the latter experiment made it possible to perform a Rosenbluth separation and a subsequent isolation of transverse parts \mathcal{R}_T of cross sections. Once inelastic background effects are removed, one is left with a simple expression for $\mathcal{R}_T^{NE} \propto [(G_M^p)^2 + (G_M^n)^2]$.

Another source of information is the asymmetry in the inclusive process $^3\text{He}(\vec{e}, e')X$ [4, 5], which requires for its analysis a complete 3-body calculation. In most of those one has neglected Final State Interactions (FSI) or relativistic kinematics [5, 6]. The present range $Q^2 \lesssim 0.6 \text{ GeV}^2$ will soon be considerably enlarged [7].

In the following we re-open the discussion on the extraction of G_M^n from QE inclusive scattering on D and other targets. There is no change in the basic understanding of those reactions. New is the much improved accuracy, for instance, with which one nowadays computes wave functions for light targets [8]. In parallel, more precise expressions for FSI have been also obtained. The above new input is here applied to analyze the total-inclusive data for light nuclei.

We base our analysis on a specific relation between nuclear and nucleon structure functions. The latter leads to the definition of the Nucleon Elastic (NE) and Nucleon Inelastic (NI) components of the inclusive cross sections for a composite target, which correspond to processes where a virtual photon leaves a struck N in its ground state, or excites it.

In our analysis we consider recent D data [9, 10], as well as older ones on ^4He [11] and D [3]. We first address inelastic contributions in the QE region. We estimate their magnitude on a model of inclusive N - Δ excitation and show that those are small compared to the QE total inclusive cross section. Next we formulate in a semi-empirical fashion stringent requirements which have to be fulfilled if total inclusive cross sections are dominated by their NE components. We find that those demands are accurately fulfilled for the recent D [9, 10] and to a somewhat lesser extent for the NE3 ^4He data [11]. In the same fashion we re-analyze separated transverse parts of the above-mentioned older D data [3] and in parallel exploit the simultaneously measured total QE inclusive cross sections, which before have not been investigated in their own right.

In the above NE parts appear all four static form factors $G_{E,M}^{p,n}(Q^2)$. Those for a proton have recently been determined with improved precision [12, 13, 14], while G_E^n is reasonably well known for $Q^2 \leq 1.6 \text{ GeV}^2$ [15]. As a consequence one can extract G_M^n from cross sections, provided those are indeed dominated by their NE components.

We show that the thus determined G_M^n are essentially independent of both the QE data points chosen for extraction,

and of the target nucleus. We discuss the sensitivity of our results to the quality of the experimental input and mention forthcoming precise data to which the presented extraction methods can be applied. Those will help to sharpen the results obtained below.

II. QUASI-ELASTIC INCLUSIVE SCATTERING.

A. Generalities.

Consider the cross section per nucleon for inclusive scattering over an angle θ of unpolarized electrons, with initial and final beam energies $E, E - \nu$. The same, relative to the Mott cross section is

$$\begin{aligned} K^A(x, Q^2) &\equiv \frac{d^2\sigma^A(E; \theta, \nu)/A}{d\Omega d\nu} \bigg/ \sigma_M(E; \theta, \nu) \\ &= \left[\frac{2xM}{Q^2} F_2^A(x, Q^2) + \frac{2}{M} F_1^A(x, Q^2) \tan^2(\theta/2) \right] \end{aligned} \quad (2.1)$$

$F_{1,2}^A(x, Q^2)$ are the nuclear SF which depend on the modulus of the squared 4-momentum transfer $q^2 = -Q^2 = -(|\mathbf{q}|^2 - \nu^2)$ and on the Bjorken variable $x = Q^2/2M\nu$. With M the nucleon mass, its range is $0 \leq x \leq A$. In order to calculate the nuclear SF, we shall exploit a previously postulated relation between nucleon and nuclear SF [16], which for isospin $I = 0$ targets reads

$$F_k^A(x, Q^2) = \int_x^A \frac{dz}{z^{2-k}} f^{PN,A}(z, Q^2) \sum_l C_{kl}(z, Q^2) \left[F_l^p\left(\frac{x}{z}, Q^2\right) + F_l^n\left(\frac{x}{z}, Q^2\right) \right] / 2 \quad (2.2)$$

The link between the SF $F_{1,2}^A$ and the nucleon SF $F_{1,2}^{N=p,n}$ (assumed to coincide with the free ones), is provided by the SF $f^{PN,A}$ of a fictitious target composed of A point-nucleons. It includes the effect of the mixing of the nucleon SF via the coefficients C_{kl} , which expression can be obtained using standard procedures [17, 18]. As usual, we take $C_{11} = 1$, $C_{12} = C_{21} = 0$, and retain only C_{22} in the expression above. In Appendix A we provide details.

Many data-analyses have been made with $f^{PN,A}$, calculated in the Plane Wave Impulse Approximation (PWIA) in terms of the single-hole spectral function [19]. We favor the Gersch-Rodriguez-Smith (GRS) theory for $f^{PN,A}$ [20], which has recently been generalized for use in the relativistic regime [21]. One of the reasons of our preference is the convergence of the GRS series to the exact $f^{PN,A}$, which is generally faster than is the case for the Impulse Series (IS). Moreover, it is more convenient to use the GRS series for a computation of FSI, which are present in $f^{PN,A}$ [16, 21, 22].

In the following we shall focus on the immediate neighborhood of the Quasi-Elastic-Peak (QEP), $|x| \approx 1$, where nucleons, as described by Eq. (2.2), are the dominant parton sources (see for instance Ref. 23).

B. Nucleon-Elastic and Inelastic components of SF.

We first consider in Eq. (2.2) the SF F_k^N of nucleons and separate those in nucleon-elastic NE and NI parts $F_k^{N,NE}, F_k^{N,NI}$ ($N = p, n$), which correspond to processes $\gamma^* + N \rightarrow N$ or $\gamma^* + N \rightarrow$ (hadrons, partons). The NE components contribute only for $x = 1$, and contain the standard combinations of static electro-magnetic form factors $G_{E,M}^N(Q^2)$ ($\eta = Q^2/(4M^2)$)

$$F_1^{N,NE}(x, Q^2) = \frac{1}{4} \delta(1-x) [(G_M^p)^2 + (G_M^n)^2], \quad (2.3)$$

$$F_2^{N,NE}(x, Q^2) = \delta(1-x) \frac{[(G_E^p)^2 + (G_E^n)^2 + \eta\{(G_M^p)^2 + (G_M^n)^2\}]}{2(1+\eta)}. \quad (2.4)$$

All except G_E^n , have in the past been assumed to be of the dipole form $G_d(Q^2) = [1 + Q^2/0.71]^{-2}$, but recent experiments have detected deviations from 1 of the following quantities [12, 13, 14]

$$\alpha_N \equiv G_M^N(Q^2)/\mu_N G_d(Q^2), \quad N = p, n, \quad (2.5)$$

$$\gamma(Q^2) \equiv \frac{\mu_p G_E^p(Q^2)}{G_M^p(Q^2)} = \frac{G_E^p(Q^2)}{\alpha_p(Q^2) G_d(Q^2)}, \quad (2.6)$$

with μ_N , the static magnetic moment of a N .

In the relevant Q^2 -range, the deviation of α_p from 1 is moderate: After reaching a maximum of ≈ 1.07 at $Q^2 \approx 2 \text{ GeV}^2$, α_p decreases and crosses the value 1 for $Q^2 \approx 5 \text{ GeV}^2$ [12, 13]. In contrast, the measured deviation of γ from 1 is far more pronounced [14]

$$\begin{aligned} \gamma &= 1 && \text{for } Q^2 \lesssim 0.3 \text{ GeV}^2, \\ &\approx [1 - 0.14(Q^2 - 0.3)] && \text{for } 0.3 \lesssim Q^2 \lesssim 5.5 \text{ GeV}^2 \end{aligned} \quad (2.7)$$

As to the NI components $F_k^{N,NI}$, for sufficiently high Q^2 we use parametrized data on $F_1^p(x, Q^2)$ [24] and $F_2^p(x, Q^2)$ [25] which are actually averages over structures, reflecting inclusive resonance excitations. Those stand out for relatively low Q^2 , but get gradually smoothed for growing Q^2 . For lack of direct information on the NI parts of the SF for a neutron are frequently approximated by

$$F_k^{n,NI}(x, Q^2) \approx F_k^{D,NI}(x, Q^2) - F_k^{p,NI}(x, Q^2); \quad k = 1, 2 \quad (2.8)$$

which is reasonable for $x \lesssim 0.3$. Only recently has $F_2^n(x, Q^2)$ for $Q^2 = 3.5 \text{ GeV}^2$ been extracted with reasonable accuracy [26].

The above division of the *nucleon* SF F_k^N in NE and NI parts determines through Eq. (2.2) corresponding components $K^{A,NE}, K^{A,NI}$ in the reduced cross section defined in Eq. (2.1). For example,

$$K^{A,NE}(x, Q^2) = \left[\frac{2xM}{Q^2} F_2^{A,NE}(x, Q^2) + \frac{2}{M} F_1^{A,NE}(x, Q^2) \tan^2(\theta/2) \right], \quad (2.9)$$

and a similar expression defines $K^{A,NI}$. Explicitly, for $I = 0$ nuclei [27]

$$\begin{aligned} F_1^{A,NE}(x, Q^2) &= \frac{f^{PN,A}(x)}{4} [(G_M^p)^2 + (G_M^n)^2] \\ &= \frac{f^{PN,A}(x)}{4} G_d^2 [(\alpha_p \mu_p)^2 + (\alpha_n \mu_n)^2], \end{aligned} \quad (2.10)$$

$$\begin{aligned} F_2^{A,NE}(x, Q^2) &= \frac{x f^{PN,A}(x)}{2(1+\eta)} C_{22}(x, Q^2) \left[(G_E^p)^2 + (G_E^n)^2 + \eta \left\{ (G_M^p)^2 + (G_M^n)^2 \right\} \right], \\ &= \frac{x f^{PN,A}(x) G_d^2}{2(1+\eta)} C_{22}(x, Q^2) \left[(\gamma_c \alpha_p)^2 + \eta \left\{ (\alpha_p \mu_p)^2 + (\alpha_n \mu_n)^2 \right\} \right], \end{aligned} \quad (2.11)$$

$$\gamma_c^2 = \gamma^2 + \left[\frac{\mu_n \eta / \alpha_p}{1 + 5.6\eta} \right]^2. \quad (2.12)$$

In. Eq. (2.12) we have used the Galster parametrization $G_E^n = \left[(\mu_n \eta G_d) / (1 + 5.6\eta) \right]^2$ [28] which approximately accounts for data for $Q^2 \lesssim (1.5 - 2.0) \text{ GeV}^2$ [15].

Using the definitions

$$\begin{aligned} u(x, Q^2) &= f^{PN,A}(x, Q^2) \alpha_p^2(Q^2) G_d^2(Q^2), \\ v(x, Q^2) &= \left[x^2 / 2(1 + \eta) \right] C_{22}(x, Q^2), \end{aligned} \quad (2.13)$$

one solves from Eqs. (2.9), (2.10) and 2.11), for the desired α_n

$$\frac{\alpha_n(Q^2)}{\alpha_p(Q^2)} = \frac{2}{\mu_n} \left[\frac{MK^{A,NE}(x, Q^2) / [2u(x, Q^2)v(x, Q^2)] - \gamma_c^2(Q^2) / 4\eta}{1 + \tan^2(\theta/2) / v(x, Q^2)} - \left(\frac{\mu_p}{2} \right)^2 \right]^{1/2}. \quad (2.14)$$

Should transverse components $\mathcal{R}_T^{A,NE} = F_1^{A,NE} / M$ be available, Eq. (2.14) for those reduces to

$$\frac{\alpha_n(Q^2)}{\alpha_p(Q^2)} = \frac{2}{\mu_n} \left[\frac{M\mathcal{R}_T^{A,NE}(x, Q^2)}{u(x, Q^2)} - \left(\frac{\mu_p}{2} \right)^2 \right]^{1/2}. \quad (2.15)$$

Next we discuss general trends of the NE, NI components as functions of x, Q^2 in the QE region [22]. The SF $f^{PN,A}$ of a nucleus, composed of point nucleons, peaks around the QEP at $x \approx 1$ ($\nu \approx Q^2/2M$), and decreases strongly with increasing $|x - 1|$. Eqs. (2.10), (2.11) then implies similar behavior of $F_k^{A,NE}$. As regards the variation with Q^2 , by far the strongest ones are due to the static form factors $G(Q^2)$ in $F_k^{A,NE}(x, Q^2)$, which approximately decrease as $\approx Q^{-4}$, while σ_M in Eq. (2.1) at constant E, θ is independent of Q^2 .

The NI parts have entirely different characteristics. Most pronounced for fixed θ is their steady increase with ν (decreasing x), causing NI parts to dominate the deep inelastic region $x < 1$. For increasing Q^2 , NI components decrease, but less rapid than do the NE ones. Ultimately NI competes with NE parts, even on the elastic side $x \geq 1$ of the QEP.

The above reasoning predicts that the reduced total cross sections for $Q^2 \geq (1.5 - 2.0) \text{ GeV}^2$ generally vary smoothly with ν . Roughly speaking, around the QEP, $\nu \approx Q^2/2M$, NI components overtake NE, which is reflected in a change of the logarithm of the slope of cross sections. The above behavior has indeed been observed for $A \geq 12$ (see Fig. 1a), for which incidentally, the normalized $f^{PN,A}$ hardly depend on A [22]. In contrast, the non-standard structure of the lightest nuclei with $A \leq 4$ (for instance reflected in the quantitatively different single- N momentum distributions), causes the normalized $f^{PN,A}(x, Q^2)$ to be much sharper peaked, than is the case for $A \geq 12$. Fig. 2 illustrates this on $f^{PN,A}(x, Q^2 = 3.0 \text{ GeV}^2)$ for D, ${}^4\text{He}$, Fe (or C, Au), whereas Fig. 3 displays the Q^2 dependence of $f^{PN,D}(x, Q^2)$.

From the above one predicts, that in medium and low Q^2 cross sections for inclusive scattering on targets with $A \leq 4$, the QEP may stand out against a smooth background. With increasing Q^2 , those peaks fade into the NI background. Both features appear confirmed by data (cf. Fig. (1b)).

We already argued that for decreasing Q^2 the NE component increases relative to the NI one. Ultimately one reaches $Q_c^2 \approx (2.0 - 2, 5) \text{ GeV}^2$, below which Eq. (2.2) is no longer reliable as a tool for a calculation of NI. Yet, when wishing to extract information from NE parts of cross sections by their isolation, one clearly needs to know the relative size of the NI background.

Another difficulty in the same Q^2 -region regards the use of parametrized, resonance-averaged F^N , which masks actual resonance structures. In fact, one may exploit inclusive resonance excitation as a model for $F_k^{A,NI}$. As is the case for the NE parts, Eqs. (2.10), (2.11), we expect that, irrespective of the relatively low Q^2 , Eq. (2.2) will properly produce the corresponding $F_k^{A,res}$ due to an isolated resonance of moderately small width. In Appendix B we present relevant material for $N \rightarrow \Delta$. Should the numerical outcome indeed prove that NI is negligibly small compared to NE, the latter can be identified with actual data, i.e. $K^{A,exp} \approx K^{A,NE}$.

III. ANALYSIS.

In the following we shall analyze the following QE data sets:

- A) Recent D-data, $E=4.045 \text{ GeV}$, $\theta = 15^\circ, 23^\circ$ [9, 10].
- B) ${}^4\text{He}$ data for $E=2.02 \text{ GeV}$, $\theta = 20^\circ$ and $E= 3.595 \text{ GeV}$, $\theta = 16^\circ, 20^\circ$ [11]. Those may well be the first QE inclusive scattering data on a nucleus, heavier than D . to be used as a source for G_M^n .
- C) Older D-data for more or less constant $Q^2 = 1.75, 2.50, 3.75 \text{ GeV}^2$ [3], which comprise total inclusive cross sections (2.14) at approximately the same x, Q^2 for various beam energies and scattering angles and Rosenbluth-separated transverse components. Those contain G_M^n only in conjunction with G_M^p . Results for \mathcal{R}_T^A have in Ref. 3 been presented as effectively originating from data with $\theta = 20^\circ$, which implies some binning of bands of Q^2 values.

We start with the NI cross sections $d^2\sigma^{A,NI}$, first estimated from inclusive Δ production (Appendix B). In Table I we both enter results for a Δ with its actual and a zero-width. One notices that the latter produces cross sections about a factor 2 lower than one with its actual width. This outcome warns against the use of an excitation amplitude into the tail of a resonance, far beyond, say, twice the width of the used Breit-Wigner amplitude (B11).

In addition of the above, we also performed a standard calculation of $F^{A,NI}$ for $Q^2 \lesssim 2.5 \text{ GeV}^2$ using parametrized, resonance-averaged F_k^N . The results are entered in the 7th column of Table I and enable a comparison with the resonance-excitation predictions. We estimate that only the entry for $Q^2 \approx 2 \text{ GeV}^2$ may be indicative of the actual size of $F^{A,NI}$.

From the results in Table I it is difficult to reach a firm conclusion regarding the size and Q^2 -dependence of the NI background $d^2\sigma^{A,N \rightarrow \Delta}$ around the QEP. Recalling that Eq. (B12) give an upper limit for $d^2\sigma^{A,NI}$, we tend to conclude that in the QE region of the considered experiments the computed Δ excitation contributions are small and presumably negligible. Nevertheless, the conclusion is not firm, and it is desirable to look for corroborative evidence, which confirms NE dominance. Only then can one safely extract G_M^n from Eq. (2.9).

Such support can actually be found in a semi-empirical fashion directly from data, specifically on the elastic side $x \gtrsim 1$, $\nu \lesssim Q^2/2M$ of the QEP, and for sufficiently small Q^2 , in addition on its adjacent inelastic side $x \lesssim 1; \nu \gtrsim$

$Q^2/2M$. In order to conclude that the data in those regions are essentially uncontaminated NE, and thus directly accessible to the extraction of G_M^n by means of Eqs. (2.9)–(2.11), the following requirements ought to be fulfilled:

i) In QE regions $x_{NI}(Q^2) \lesssim x \lesssim 1.1$, with $x_{NI}(Q^2)$ the x -value (< 1), where the NI part about overtakes the NE component, the cross sections should follow the computed bell-shaped x -dependence of $f^{PN,A}(x, Q^2)$, with computed target A and x, Q^2 dependence.

ii) Extracted $\alpha_n(Q^2)$ from either Eq. (2.14) or (2.15) should not depend on the x -values chosen for the extraction.

iii) $\alpha_n(Q^2)$ should not depend on the target in which the neutron is embedded.

With $f^{PN,A}$ the source of the strongest variation with x , requirements i) and ii) demand that $K^{A,NE}(x, Q^2)/u(x, Q^2)v(x, Q^2)$ in Eq. (2.9) be x -independent, and moreover, that $\tan^2(\theta/2)/v(x, Q^2) \ll 1$. The same nuclear SF $f^{PN,A}$ carries the A -dependence, which we recall, is most pronounced for $A \leq 4$: the ratio $K^{A,NE}/f^{PN,A}$ in Eq. (2.9) should be A -independent.

The above conditions are quite stringent and lean heavily on the central role played by $f^{PN,A}$. Of course, it is always possible to fit one or two points on the elastic side of the QEP ($x \gtrsim 1$), whether or not the cross sections do contain some NI part in addition to the NE component. However, since NI parts grow with decreasing x (increasing ν), a fit of NE based on one or two points, cannot possibly hide a NI component over an *extended* interval $x_{NI} \lesssim x \lesssim 1.1$.

The above is most expediently tested on QE data which are represented on a linear scale. Figs. 4 and 5 show that criterion i) is very well met for recent, high-quality D data in the elastic neighborhood of the QEP. As a result we could extract, for a range of selected data points, $\alpha_n(Q^2; x_k)$, and from those an unbiased average $\alpha_n(Q^2) \equiv \langle \alpha_n(Q^2) \rangle$ and an error of the mean.

For x decreasing into the inelastic region of the QEP (increasing ν), differences emerge between the measured and computed NE cross sections for fixed $\alpha_n(Q^2)$. Those reflect the growing importance of NI parts, for $x \lesssim x_{NI}$ and increasing with Q^2 .

The very quality of the fit makes one wonder why, for the stated average α_n , the maxima of the two D cross sections is off by 3-5 %. We probed, sometimes substantially larger α_n and the result for those is common to all cases to be discussed: even a 10% increase in α_n hardly affects the NE wings and only moderately changes the peak area. Those bridge only a small part of the discrepancy there, while the error from the mean generally grows. It seems more likely that, what seems to be a tiny misfit at the QEP, is actually the onset of NI at about the same ν . In line with expectations, those are smooth in ν .

It is of course desirable to have an error estimate $\Delta\alpha_n(Q^2, x_k)$ due to the systematic errors in the cross sections. In spite of the fact that the latter are only of the order of a few %, the resulting averaged error estimates $\langle \Delta\alpha_n(Q^2, x_k) \rangle$ may be large fractions of the average $\langle \alpha_n(Q^2, x_k) \rangle$. Clearly, the desired error estimates require far smaller systematic errors on the data than are presently available. The above failure actually contains information: provided the data are smooth and have a small error of the mean, the method of extraction of $\alpha_n(Q^2, x_k)$ and its average is quite sensitive to the central data. This is borne out by the above D data sets A).

At this point we make a digression and report on an attempt to fit the $\theta = 23^\circ$ D data, with $f^{PN,D}$ for $\theta = 15^\circ$, or alternatively with a Q^2 -independent $f^{PN,D}$. The result, the dashed curve in Fig. 5, manifestly produces a far worse fit than the the drawn line for $f^{PN,A}$ with the Q^2 appropriate to $\theta = 23^\circ$. The above supports (but does not prove) the assumption that the SF $f^{PN,A}$ in the link (2.2) is Q^2 -dependent, as its interpretation as a SF of a nucleus demands. It runs counter the claim that $f^{PN,A}$ is Q^2 -independent, which holds in the PWIA (see for instance Ref. 31), but not for the GRS theory used above.

Next we discuss the above mentioned older ^4He data sets [11]. As a comparison of Figs. 4,5 and Figs. 6–8 shows, the quality of the He data is inferior to those for D and consequently one cannot expect a similar precision for α_n , as obtained from the above D data.

An additional complication is the non-negligible mixing of nucleon SF in F^A , which is primarily determined by C_{22} , given by Eq. (A10). Although qualitatively understood, any evaluation amounts in practice to an approximation.

B1) $E = 2.02$ GeV, $\theta = 20^\circ$: maxima of the theoretical and experimental cross sections coincide. The data appear to fall into two groups, with at $\nu \approx 0.225$ GeV an apparent, non-smooth transition (cf. Fig. 6). Only an exceptionally large α_n can accommodate data on the elastic side of that point, but those will not simultaneously fit the QEP region. On these grounds we disregarded the former. This leaves only a small sample of data points in the immediate elastic neighborhood of the QEP.

Fortunately, for very low $Q^2 \approx 0.45$ GeV², NE is still dominant in some range on the inelastic side of the QEP. Indeed, adding to the first 4 data points one or two more with $\nu \geq 0.225$ GeV, the average α_n changes by only 1%, slightly diminishing the error of the mean. Ultimately (for $\nu \gtrsim 0.3$ GeV) the NI overtakes.

We illustrate the above by comparing data with NE predictions for three values of $\alpha_n=0.90,0.98,1.06$ in Fig. 6. Those show the above-mentioned impossibility to get a fit including additional low ν points. In particular not by a shift of the theoretical curve, allegedly representing the effect of an average separation energy: recoil has been included in calculations [32].

B2) $E = 3.6$ GeV, $\theta = 16^\circ$: maxima of the theoretical and experimental cross sections coincide. Those are the

smoothest data amongst the three He sets, but again, the more elastic points cannot be accommodated together with the QEP region (see Fig. 7). Curves are for $\alpha_n = 1.00, 1.06, 1.12$.

B3) $E = 3.6$ GeV, $\theta = 20^\circ$: maxima of the theoretical and experimental cross sections do not coincide. Again the data appear to lie on two smooth, disjoint curves and moreover show substantial noise around the QEP, continuing into the near-NI region (see Fig. 8). Curves are for $\alpha_n = 0.96, 1.02, 1.08$. The analysis comprises 6-8 points with $\nu \geq 0.615$ GeV. Addition of the 7th and 8th point on the inelastic side of the QEP reduces the average by a mere 1% and 2% respectively. For all three cases, unbiased averages are close to the central α_n shown, and are entered in Table II.

We only briefly mention the total cross sections and separated transverse D data of Lung [3] (sets C)). Part of those are for medium, and part for larger Q^2 : all reduced data follow the theoretical predictions, but only to about 10% accuracy. We note that for all Q^2 the data are given only to two decimals. Therefore, in spite of the approximately fulfilled requirement i), insufficient accuracy hampers the drawing of sharper conclusions.

To the above one may add that the extracted results may well be affected by the precision of the Rosenbluth separation (cf. Figs. 55 and Table 22 in Lung's PhD Thesis [3]). The latter appears to have been renormalized to one nominal $\theta = 20^\circ$, which implies some binning. Consequently, in spite of the fact that the Rosenbluth-separated \mathcal{R}_T contains a simpler form for G_M^n than does the total cross sections, we consider the latter to be a competitive and fiducial tool for extraction.

Table II summarizes our results for $\alpha_n(Q^2)$. Column 1 indicates the targets for which total QE inclusive cross sections have been analyzed, whereas the same for separated transverse data are denoted by \mathcal{R}_T . Columns 2-5 contain the beam energies, the scattering angles, ranges of the considered Bjorken x on the elastic side up to, and just over the QEP, and the corresponding ranges of Q^2 . The separated \mathcal{R}_T^A are all for fixed Q^2 at the QE peak and correspond to renormalized energies E and fixed $\theta = 20^\circ$ [3]. The 6-th column gives ranges of the point-nucleon nuclear SF, with in parenthesis values at the QEP. The last column presents the values of the extracted $\langle\alpha_n(Q^2)\rangle$, which measures the deviation of $G_M^n(Q^2)/\mu_n$ from a dipole form factor. As discussed above, we only give errors of the mean values and do not include systematic errors in the underlying data. $\mathcal{R}_T^{D,NE}$ between parenthesis in the last column are the results of Lung [3].

The results in Table II and a few earlier values of $\alpha_n(Q^2)$ are shown in Fig. 9. The values, obtained in the present analysis are seen to agree amongst themselves and, within the experimental accuracy with information from other sources.

IV. SUMMARY AND CONCLUSIONS.

We have analyzed QE inclusive scattering on D and ^4He . From the general behavior of NE components, where a nucleon in the medium absorbs a virtual photon without being excited, we concluded that one should observe an outstanding QEP in moderate Q^2 cross sections for inclusive scattering on the lightest targets. For non-separated cross sections, those NE parts contain all four static form factors, as well as $f^{PN,A}(x, Q^2)$, the computed SF of a nucleus composed of point-nucleons. With knowledge of $G_{E,M}^p$ and information on G_E^n , the NE component of the cross section is a measure for $\alpha_n(Q^2) = G_M^n(Q^2)/\mu_n G_d(Q^2)$.

In order to assess to what extent the experimental QE cross sections are well represented by the uncontaminated NE component, one has to know the size of the NI background, relative to NE. We first assumed that the dominant NI parts are generated by the excitation of Δ resonances. In general their contributions on the elastic side of the QEP are small. However, those NI estimates for the QE region in the tail of the Breit-Wigner excitation amplitude are presumably not sufficiently precise.

In a far more reliable, semi-empirical approach, one compares the x -dependence of the reduced cross section data in the immediate region of the QEP with the theoretical prediction, Eqs. (2.9)–(2.11) for a purely NE component. Our results:

1) The values $\alpha_n(Q^2; x_k)$, extracted from the QE part of recent D data, show little variation with x_k and an unbiased average $\alpha_n(Q^2) \equiv \langle\alpha_n(Q^2)\rangle$ produces excellent fits to the recent D data. As expected, deviations due to NI appear on the inelastic side of the QEP and grow with ν and Q^2 .

2) The poorer quality of the He data bars an equally clean result for the He data. Nevertheless we could extract from those reasonable α_n .

3) We re-analyzed Lung's non-separated D cross sections for similar x, Q^2 , but different E, θ . For increasing Q^2 , the relative weight of G_E^n grows, but simultaneously, information on G_E^n becomes increasingly scant. We therefore only analyzed total cross sections for the lowest $Q^2 = 1.75, 2.50$ GeV² of the above experiment.

4) The same experiment with varied kinematics provides \mathcal{R}_T , in principle the simplest source of G_M^n from inclusive QE scattering. One expects the above source and unseparated data to produce the same G_M^n . The entries in Table II bear this out for $Q^2 = 1.75$ GeV², while Lung's value from \mathcal{R}_T^{NE} for $Q^2 = 2.5$ GeV² somewhat exceeds our result.

However, for the larger measured Q^2 , our analysis seems to show a stronger downward trend of $\alpha_n(Q^2)$ for growing Q^2 than reported by Lung.

It is clear from our analysis that the extracted $\alpha_n(Q^2)$ are sensitive to the precision of the input. For instance, a 5% changes in cross sections may produce ten times larger relative changes in $\alpha_n(Q^2)$. The same prevents the allocation of systematic 'errors' to extracted α_n , due to the same in the data.

We conclude that medium Q^2 QE inclusive scattering on light nuclei provide an accurate tool to determine G_M^n , with as single most important source of lack of accuracy, the same in the underlying data.

Until recently we were rather pessimistic as to prospects for new information. It appears however, that new JLab data on ${}^3\text{He}$ have already been taken, D data are forthcoming, while experiments on ${}^4\text{He}$ have been approved. Once analyzed, those data will be directly accessible to the above analysis and promise to sharpen the predictions in this communication, in particular for ${}^4\text{He}$.

In parallel, $D(e, e'p)$, $D(e, e'n)$ measurements will extend reliable information on α_n over a wider Q^2 range [37]. This will enable to establish whether $\alpha_p(Q^2)$ and $\alpha_n(Q^2)$ continue to behave similarly as function of Q^2 .

V. ACKNOWLEDGEMENTS.

ASR has profited from discussions with several experimentalists at JLab, in particular with Haiyan Gao, Cynthia Keppel and Doug Higinbotham and others. ASR thanks Jian-Ping Ling for emphasizing the need to ascertain the role of resonance tails in the QE region. Allison Lung supported our re-analyses of her NE11 data and Paul Stoker helped in locating inclusive Δ production data.

APPENDIX A: DISCUSSION OF THE MIXING COEFFICIENT IN THE GRS THEORY

The sensitivity of the extracted G_M^n from inclusive scattering data, in particular for low Q^2 , calls for scrutiny in the handling of tools for analysis. A delicate aspect of the theory used here concerns the mixing coefficients entering Eq. (2.1). All treatments and applications we know of are based on a comparison of hadron tensors of the target and of an isolated nucleon in the PWIA of the full IS [17, 18]. Those tensors contain invariants $p \cdot q$ and $p^A \cdot q$, with p , p^A , the 4-momenta of the struck N and the target, and are related by the single-hole spectral function S of the target

$$W^{A,\mu\nu}(p^A, p^A \cdot q) = \int \frac{d^4p}{(2\pi)^4} S(p) W^{N,\mu\nu}(p, p \cdot q), \quad (\text{A1})$$

Expressing the hadron tensors by use of the invariant SF F_k , one obtains

$$F_k^A(x, Q^2) = \int \frac{d^4p}{(2\pi)^4} S(p) \sum_{\ell=1,2} C_{k\ell}(p, \nu, |\mathbf{q}|) F_k^N(\tilde{x}, Q^2), \quad (\text{A2})$$

with $\tilde{x} = Q^2/2M\nu' + p^2 - M^2$; $\nu' = (p_0\nu - p_z|\mathbf{q}|)/M$ [17, 18]. In particular the dominant coefficient reads

$$C_{22}(p, \nu, |\mathbf{q}|) = \left[1 + \frac{Q^2 p_z}{|\mathbf{q}|\nu' M} \right]^2 + \frac{Q^2}{|\mathbf{q}|^2} \left[\frac{\nu}{\nu'} \right]^2 \frac{[p_\perp]^2}{2M^2}, \quad (\text{A3})$$

where p_z is the component of the 3-momentum \mathbf{p} of the struck nucleon along \mathbf{q} , while $p_\perp^2 = |\mathbf{p}|^2 - p_z^2$. One shows that the mixing coefficients $C_{11} = 1$ and $C_{21} = 0$ [17, 18], while C_{12} is negligibly small.

When using the GRS theory one has to reduce the 4-dimensional integration in Eq. (A1) to a 3-dimensional one. In a standard approximation one assumes the spectator nucleus to be on its mass shell, which determines p_0 by energy conservation in the vertex $(A, A-1_n, N)$. Thus in the target rest frame

$$\begin{aligned} p_0 &= M_A - \sqrt{|\mathbf{p}|^2 + [M_{A-1}^n]^2} \\ &\approx M_A - M_{A-1}^n - |\mathbf{p}|^2/2M_{A-1}^n, \end{aligned} \quad (\text{A4})$$

where M_{A-1}^n is the mass of the $A-1$ system in the n -excited state and M_A the mass of the target in its ground state.

There is also no unique way to determine p_z and we chose the covariant Gurvitz prescription [33]: before and after absorption of the virtual photon, the nucleon is to equal measure off its mass-shell, i.e. $p^2 = (p+q)^2$ and consequently

$$p_z = \frac{\nu}{|\mathbf{q}|} \left(p_0 - \frac{Q^2}{2\nu} \right) = \frac{\nu}{|\mathbf{q}|} (p_0 - Mx) \quad (\text{A5})$$

The above and Eq. (A4) for p_z, p_0 are intimately related to a covariant GRS approach [16, 33] and are used in Eq. (A3).

To obtain the coefficient C_{22} entering Eq. (2.2), one starts from the structure function of a nucleus composed by point-nucleons, which in the GRS theory is first expressed in terms of the variable $|\mathbf{q}|, y_G$ [16]. That function is written as a lowest order term, supplemented by a FSI term

$$\mathcal{F}^{GRS}(y_G, |\mathbf{q}|) = \mathcal{F}_0^{GRS}(y_G, |\mathbf{q}|) + \mathcal{F}_{FSI}^{GRS}(y_G, |\mathbf{q}|) . \quad (\text{A6})$$

Above, y_G is the Gurvitz scaling variable [16]

$$y_G = \frac{M}{|\mathbf{q}|} \left[\nu \left(1 - \frac{\Delta}{M} \right) - \frac{Q^2}{2M} \right] \quad (\text{A7})$$

with Δ the smallest separation energy of the $(A - 1)$ nucleus from the target. We only correct $\mathcal{F}_0^{GRS}(y_G, |\mathbf{q}|)$

$$\mathcal{F}_0^{GRS}(y_G, |\mathbf{q}|) \rightarrow \mathcal{F}_{0,kl}^{GRS}(y_G, |\mathbf{q}|) = \int \frac{d^4p}{(2\pi)^4} S(p) \delta[2\nu p_0 - 2p_z |\mathbf{q}| - Q^2] \mathcal{C}_{kl}(p, \nu, |\mathbf{q}|) \quad (\text{A8})$$

The point-nucleon nuclear SF $f^{PN,A}(x, Q^2)$ is then obtained by expressing the function \mathcal{F} for the case $kl = 11$ in terms of the kinematic variables (x, Q^2) [22], namely

$$f^{PN,A}(x, Q^2) \equiv \mathcal{F}_{0,11}^{GRS}(y_G, |\mathbf{q}|) + \mathcal{F}_{FSI}^{GRS}(y_G, |\mathbf{q}|) , \quad (\text{A9})$$

where we recall that $\mathcal{C}_{11} = 1$. Finally, the coefficient C_{22} in Eq. (2.2) is defined as

$$C_{22}(x, Q^2) f^{PN,A}(x, Q^2) \equiv \mathcal{F}_{0,22}^{GRS}(y_G, |\mathbf{q}|) + \mathcal{F}_{FSI}^{GRS}(y_G, |\mathbf{q}|) . \quad (\text{A10})$$

APPENDIX B: $N \rightarrow \Delta$ PART OF INCLUSIVE NI CROSS SECTION

In the following we discuss the NI background in the QE region, as due to inclusive electro-excitation of the nearest Δ -resonance. Its cross section for a proton is

$$d^2\sigma^{p,NI} \rightarrow d^2\sigma^{p,\Delta} \approx \sigma_M F_2^{p,\Delta} / \nu \quad (\text{B1})$$

$$F_2^{p,\Delta}(x, Q^2) = \frac{Q^2}{x} \mathcal{N}(\Gamma_\Delta) \mathcal{G}_{p\Delta}^2(Q^2) \frac{M_\Delta \Gamma_\Delta / \pi}{[Q^2(1/x - 1) - (M_\Delta^2 - M^2)]^2 + [M_\Delta \Gamma_\Delta]^2} \quad (\text{B2})$$

Since all data are for forward angles, it suffices to consider only F_2 . $\mathcal{G}_{p\Delta}$ denotes a transition form factor to be given below and the number $\mathcal{N}(\Gamma_\Delta)$ in Eq. (B2) accounts for a proper normalization of the nearly-elastic resonance amplitude.

Total cross section data are frequently expressed in terms of those for transverse and longitudinal virtual photons (see for instance Ref. 34)

$$\sigma = \gamma_t(\sigma_t + \epsilon\sigma_l) \quad (\text{B3})$$

$$\epsilon^{-1}(E; \nu, Q^2) = 1 + \frac{|\mathbf{q}|^2}{Q^2} \tan^2(\theta/2), \quad (\text{B4})$$

with

$$\gamma_t(E; \nu, Q^2) = \sigma_M(E; \nu, Q^2) \frac{Q^2}{4\pi^2 \alpha |\mathbf{q}| \epsilon(E; \nu, Q^2)}, \quad (\text{B5})$$

$$\approx \frac{\alpha}{\pi^2} \frac{(E - \nu)^2}{|\mathbf{q}| Q^2} \quad (\text{B6})$$

the flux of virtual photons. For small θ one approximates $\epsilon \approx \epsilon^{-1} \approx 1$, to be used in Eq. (B4).

As regards the transition form factor in Eq. (B2), we assume it to be of the form (cf. Eqs. (2.10), (2.11)) for NE).

$$\begin{aligned} \mathcal{G}_{p\Delta}(Q^2) &= \mu_{p\Delta} G_{p\Delta}(Q^2) \\ G_{p\Delta}(Q^2) &= \left[\frac{1}{1 + Q^2/Q_{p\Delta}^2} \right]^2, \end{aligned} \quad (\text{B7})$$

with $\mu_{p\Delta}$, some effective transition magnetic moment and the reduced transition form factor $G_{p\Delta}$ of a dipole form. The parameters in Eq. (B7) are estimated by a comparison of small θ data for reduced cross sections with Eq. (B2)

$$\Sigma^{p,\Delta} = d^2\sigma^{p,\Delta}/\gamma_t$$

In particular at the top of the resonance

$$\Sigma^{p,\Delta,\max} \approx [\sigma_M F_2^{p,\Delta,\max}/\nu]/\gamma_t \approx 8\pi\alpha \frac{|\mathbf{q}|}{Q^2} \frac{M}{M_\Delta \Gamma_\Delta} [\mu_{p\Delta} G_{p\Delta}(Q^2)]^2 \quad (\text{B8})$$

From data for $Q^2=0.5, 1.0, 2.0$ GeV² (Figs. 12, 13, 14 in Ref.[35]), we extracted $Q_{p\Delta}^2 \approx 2.7$ GeV², $\mu_{p\Delta}^2 \approx 0.9$. Those values have been used in Eq. (B7) for all relevant Q^2 .

No such information exists for the neutron. However, guided by the behavior of the nucleon SF, averaged over resonances, $\langle F_2^p \rangle, \langle F_2^n \rangle$ (see for instance Ref. [36]), it is reasonable to assume that

$$\left(F_2^{p\Delta} + F_2^{n\Delta} \right) / 2 \lesssim F_2^{p\Delta} \quad (\text{B9})$$

The above suffices to compute $F_2^{A,\Delta}$ from Eq. (2.2)

$$F_2^{A,\Delta}(x, Q^2) = \frac{Q^2}{x} [\mu_{p\Delta} G_{p\Delta}(Q^2)]^2 I^{A,\Delta}(x, Q^2; \Gamma_\Delta) \quad (\text{B10})$$

$$I^{A,\Delta}(x, Q^2; \Gamma_\Delta) = \mathcal{N}(\Gamma_\Delta) \left(\frac{M_\Delta \Gamma_\Delta}{\pi} \right) \int_x^A dz \frac{z f^{PN,A}(z, Q^2) C_{22}(z, Q^2)}{[Q^2(z/x - 1) - (M_\Delta^2 - M^2)]^2 + (M_\Delta \Gamma_\Delta)^2} \quad (\text{B11})$$

Finally, the corresponding nuclear QE inclusive Δ excitation cross section reads

$$\frac{d^2\sigma^{A,\Delta}(E; \theta, \nu)/A}{d\Omega d\nu} \approx (2M)\sigma_M(E; \theta, \nu) [\mu_{p\Delta} G_{p\Delta}(Q^2)]^2 I^{A,\Delta}(x, Q^2; \Gamma_\Delta) \quad (\text{B12})$$

$$\approx \frac{2Mx}{Q^2} \sigma_M(E; \theta, \nu) [\mu_{p\Delta} G_{p\Delta}(Q^2)]^2 (x/x_\Delta) f^{PN,A}(x/x_\Delta, Q^2) \quad (\text{B13})$$

$$x_\Delta(Q^2) = \left[1 + \frac{M_R^2 - M^2}{Q^2} \right]^{-1} \quad (\text{B14})$$

with $x_\Delta(Q^2)$ the value of the Bjorken variable at the resonance peak. Eq. (B13) is the zero-width limit of (B12), which resembles the NE part, if $M_R \rightarrow M$, and thus $x_\Delta(Q^2) \rightarrow 1$. The same limit of x_Δ is obtained for $Q^2 \rightarrow \infty$, corresponding to the resonance position in $x = 1$, ultimately coinciding with the QEP.

For small, medium Q^2 , $1/x_\Delta$ is substantially larger than 1, i.e. the resonance peak is far from the QE region. In that case, the QEP region $x \approx 1$ corresponds to the tail of $f^{PN,A}$, far from its maximum value $f^{PN,A}(x \approx 1, Q^2)$, and consequently $d^2\sigma^{A,\Delta}$ is expected to be small. For increasing values of Q^2 , however, the resonance peak moves closer and closer to the QEP and the NI contribution to the total cross section can become there quite sizable.

-
- [1] H. Anklin *et al*, Phys. Lett. B336, 313 (1994); *ibid* B428, 248 (1998); E.E.W. Bruins *et al* Phys. Rev. Lett. 75, 21 (1995).
 - [2] G. Kubon *et al*, Phys. Lett. B524, 26 (2002).
 - [3] A. Lung *et al*, Phys. Rev. Lett. 70, 718 (1993); Ph.D. thesis, The American University, Washington D.C., 1992.
 - [4] H. Gao *et al*, Phys. Rev. C 50, R546 (1994).
 - [5] W. Xu *et al*, Phys. Rev. Lett. 85, 2900 (2000); F. Xiong *et al*, Phys. Rev. Lett 87, 24250 (2002); W. Xu *et al*, Phys. Rev. C 67, 012201 (2003).
 - [6] J. Golak *et al*, Phys. Rev. C 66, 024008 (2002)
 - [7] M. Jones, private communication.
 - [8] H. Kamada *et al*, Phys. Rev. C 64, 044001 (2001).
 - [9] J. Arrington, private communication.
 - [10] I. Niculescu *et al*. Phys. Rev. Lett. 85, 1182 (2000).
 - [11] D.B. Day *et al*, Phys. Rev. C 48, 1849 (1993).

- [12] A.F. Sill *et al*, Phys. Rev. D 48, 29 (1993); L. Andivahis *et al*, Phys. Rev. D50, 549 (1994).
- [13] E. Brash, A. Kozlov, Sh. Li, G.M. Huber, Phys. Rev. C 65, 051001 (2002).
- [14] M. Jones *et al*, Phys. Rev. Lett. 84, 1398 (2000); Third Workshop on 'Perspective in Hadronic Physics' Trieste 2001, IT; to be published; O. Gayou *et al*, Phys. Rev. C64, 038202 (2001).
- [15] R. Schiavilla and I. Sick, Phys. Rev. C 64, 041002(R) (2001).
- [16] S.A. Gurvitz and A.S. Rinat, TR-PR-93-77/ WIS-93/97/Oct-PH; Progress in Nuclear and Particle Physics, Vol. 34, 245 (1995).
- [17] G.B. West, Ann. of Phys. (NY) 74, 646 (1972); W.B. Atwood and G.B. West, Phys. Rev. D7, 773 (1973).
- [18] M.M. Sargsian, S. Simula and M.I. Strikman, nucl-th/0105052.
- [19] See for instance: C. Ciofi degli Atti, E. Pace and G. Salme, Phys. Rev. C 43, 1155 (1991).
- [20] H. Gersch, L.J. Rodriguez and Phil N. Smith, Phys. Rev. A5, 1347 (1973).
- [21] S.A. Gurvitz and A.S. Rinat, Phys. Rev. C 65, 024310 (2002).
- [22] A.S. Rinat and M.F. Taragin, Nucl. Phys. A598, 349 (1996); *ibid* A620, 412 (1997); Erratum: *ibid* A623, 773 (1997); Phys. Rev. C 60, 044601 (1999).
- [23] C.H. Llewelyn Smith, Phys. Lett. B 128 (1983) 107; M. Ericson and A.W. Thomas, *ibid* p. 112.
- [24] A. Bodek and J.L. Ritchie, Phys. Rev. D23, 1070 (1981)
- [25] P. Amadrauz *et al*, Phys. Lett. B295, 159 (1992); M. Arneodo *et al*, *ibid* B364, 107 (1995)
- [26] A.S.Rinat and M.F. Taragin, Phys. Lett. 551, 284 (2003).
- [27] A.S. Rinat and M.F. Taragin, Phys. Rev. C 62, 034602 (2000).
- [28] S. Galster *et al*, Nucl. Phys. B32, 221 (1971).
- [29] J. Arrington *et al*. Phys. Rev. Lett. 82, 2056 (1999).
- [30] A.S. Rinat and M.F. Taragin, Phys. Rev. C 65, 042201(R) (2001).
- [31] R.L. Jaffe, Nucl. Phys. A478, 3c (1988); R.P. Bickerstaff and A.W. Thomas, J. Phys. G 15, 1523 (1989).
- [32] M. Viviani, A. Kievsky and A.S. Rinat, nucl-th/0111049, Phys. Rev. C67, 034003 (2003).
- [33] S.A. Gurvitz, Phys. Rev. C 42, 2653 (1990).
- [34] P.J. Mulders, Phys. Reports, 185, 83 (1990).
- [35] F.W. Brasse *et al*, Nucl. Phys. B 110, 413 (1976).
- [36] E.D. Bloom and F.J. Gilman, Phys. Rev. Lett. 25, 1140 (1970); Phys. Rev. D 4, 2901 (1971); I. Niculescu *et al*, Phys. Rev. Lett. 85, 1186 (2000).
- [37] W. Brooks, private communication.

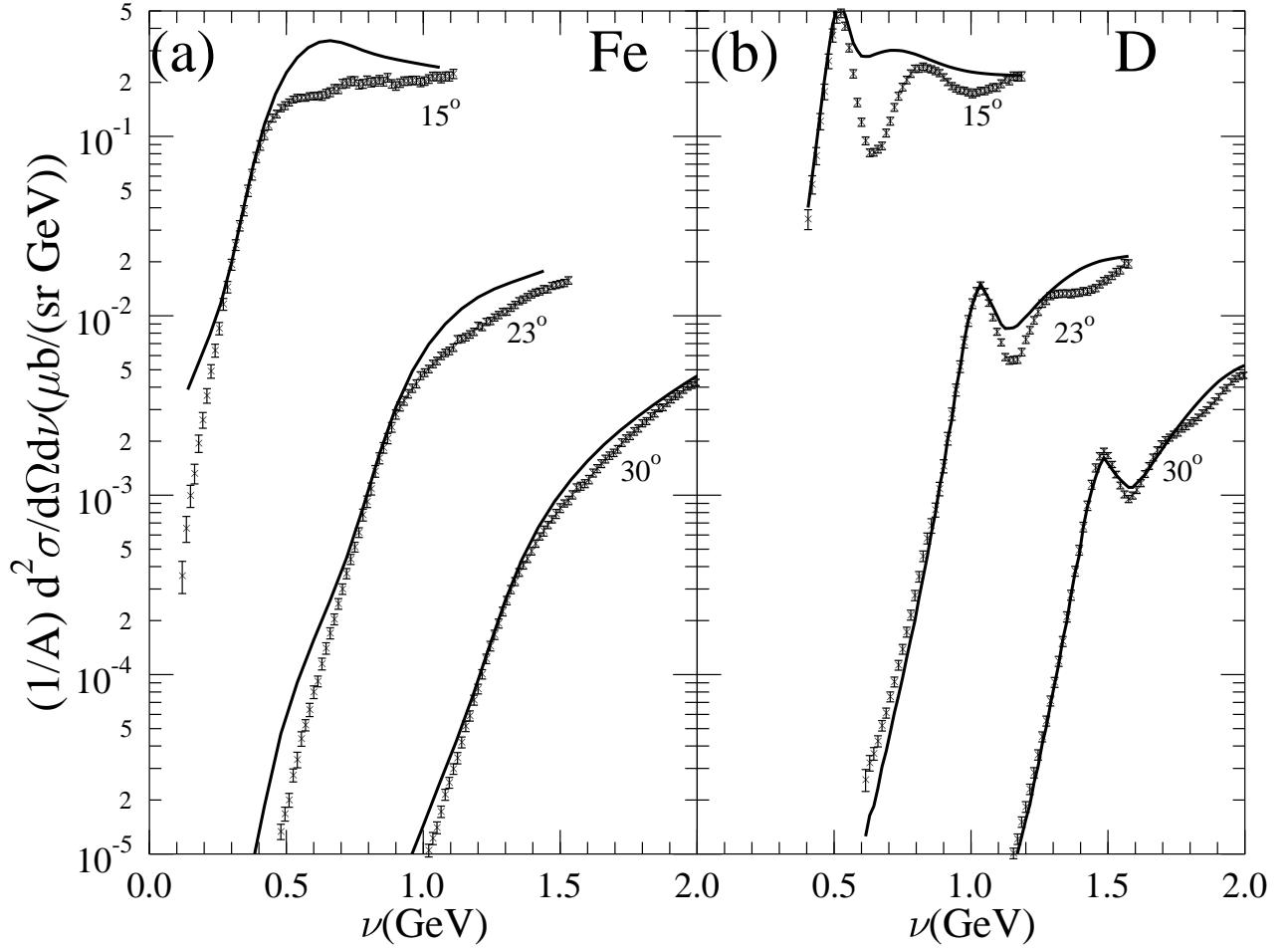


FIG. 1: (a) Data [29] and calculated [22] QEP cross sections for inclusive scattering of $E = 4.045$ GeV electrons on Fe through $\theta = 15^\circ, 23^\circ$ and 30° . (b) Same as in (a) for D; data are from [9, 30]

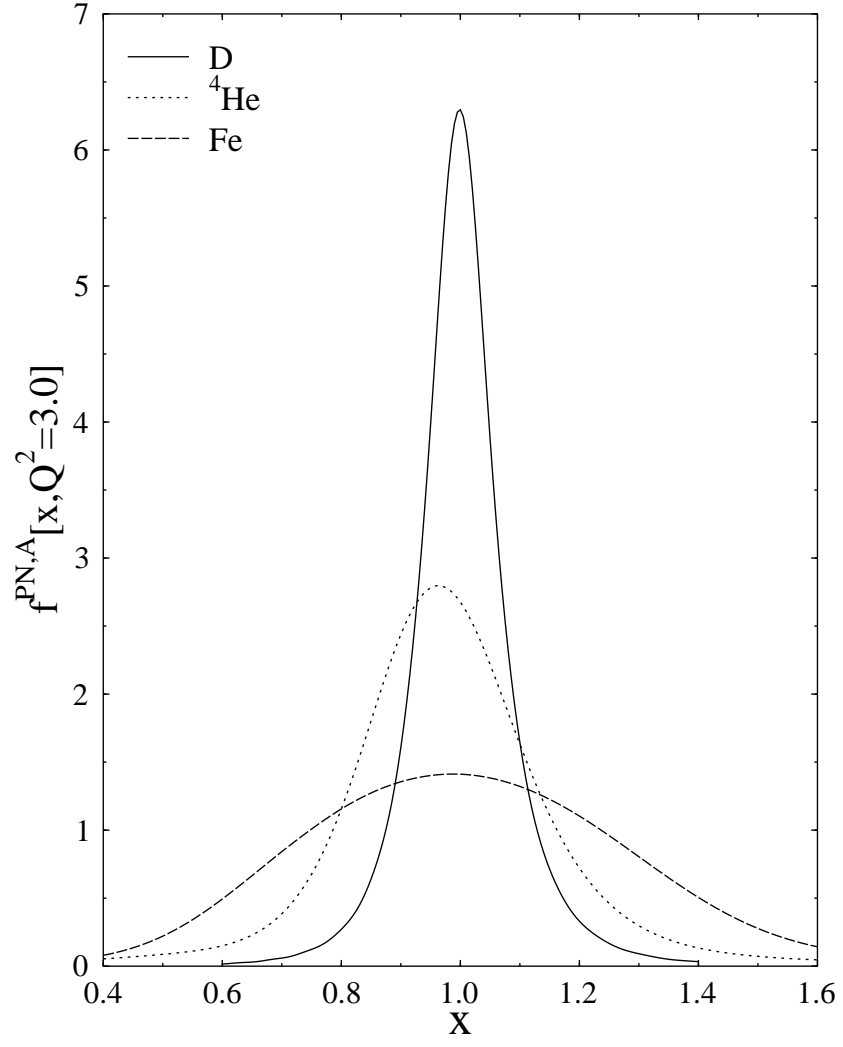


FIG. 2: Comparison of $f^{PN,A}(x, Q^2 = 3.0 \text{ GeV}^2)$ for D, ${}^4\text{He}$, Fe.

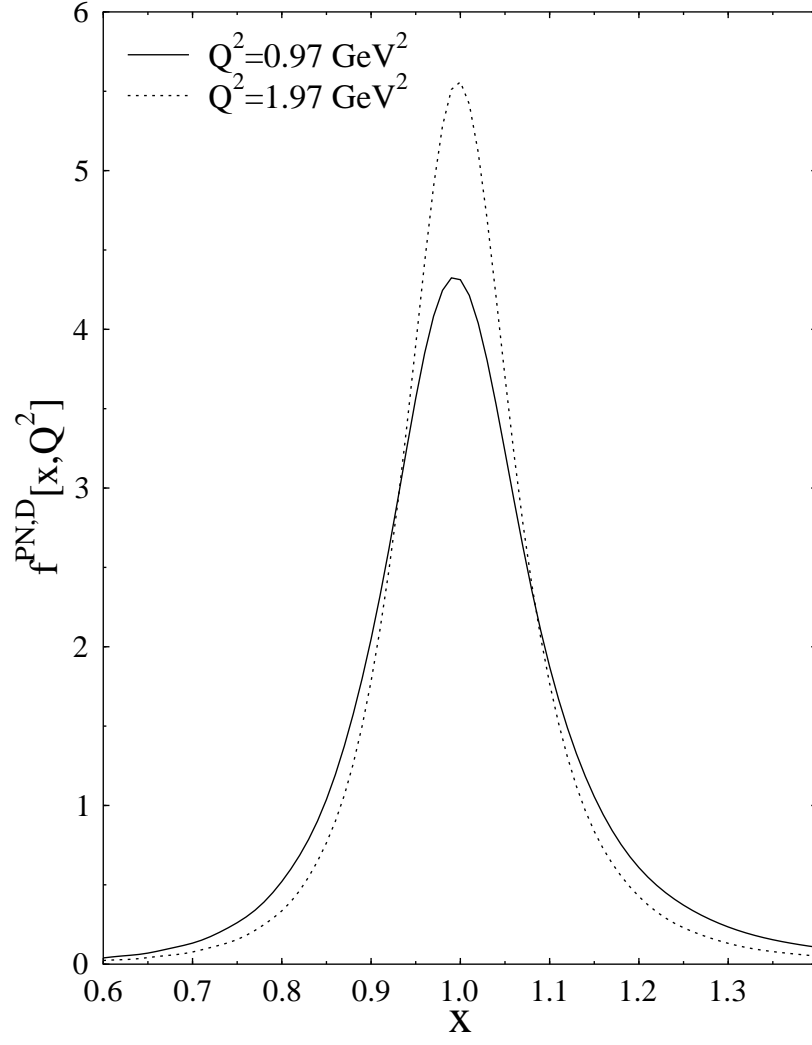


FIG. 3: The SF $f^{PN,D}(x, Q^2)$ for $Q^2 = 0.972, 1.94 \text{ GeV}^2$.

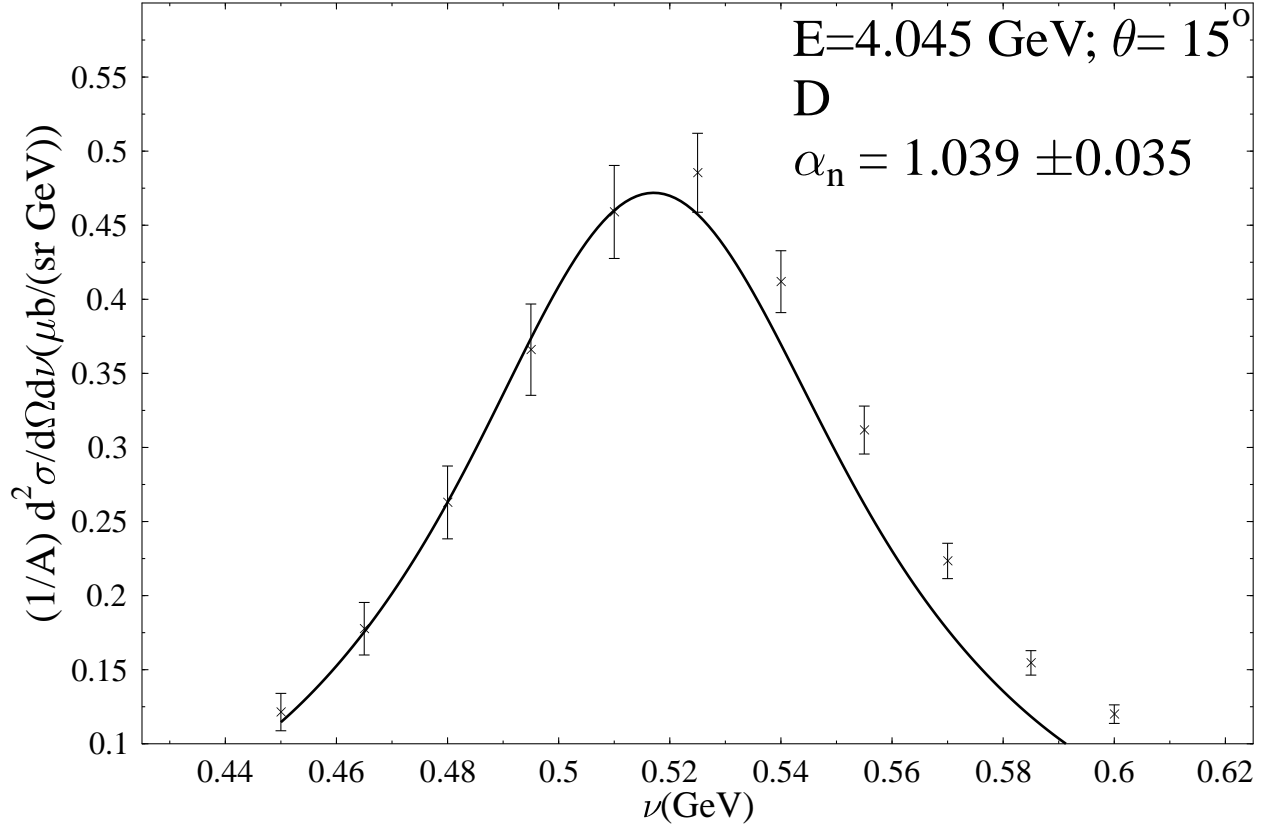


FIG. 4: Cross section for QE inclusive scattering of $E = 4.045 \text{ GeV}$ electrons on D for $\theta = 15^\circ$. The drawn line is the theoretical NE cross section for $\alpha_n = 1.039$.

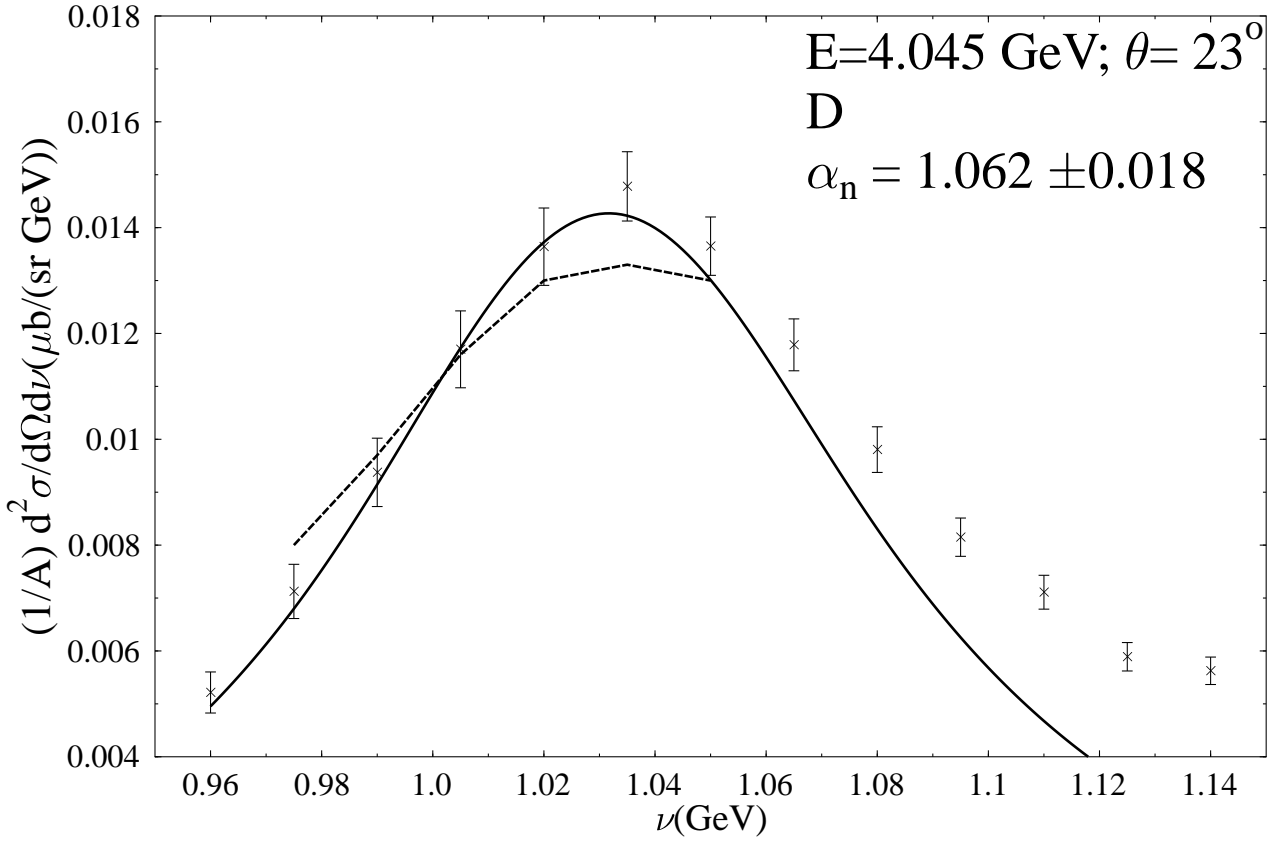


FIG. 5: The same as in Fig. 4 for $\theta = 23^\circ$. The drawn line is the theoretical NE cross section for $Q^2 = 1.94 \text{ GeV}^2$ and $\alpha_n = 1.062$. The dotted line represents the result of a calculation with the SF $f^{P^{N,D}}(x, Q^2 = 0.972 \text{ GeV}^2)$, instead of the same with the value $Q^2 = 1.94 \text{ GeV}^2$, pertinent to this case $\theta = 23^\circ$.

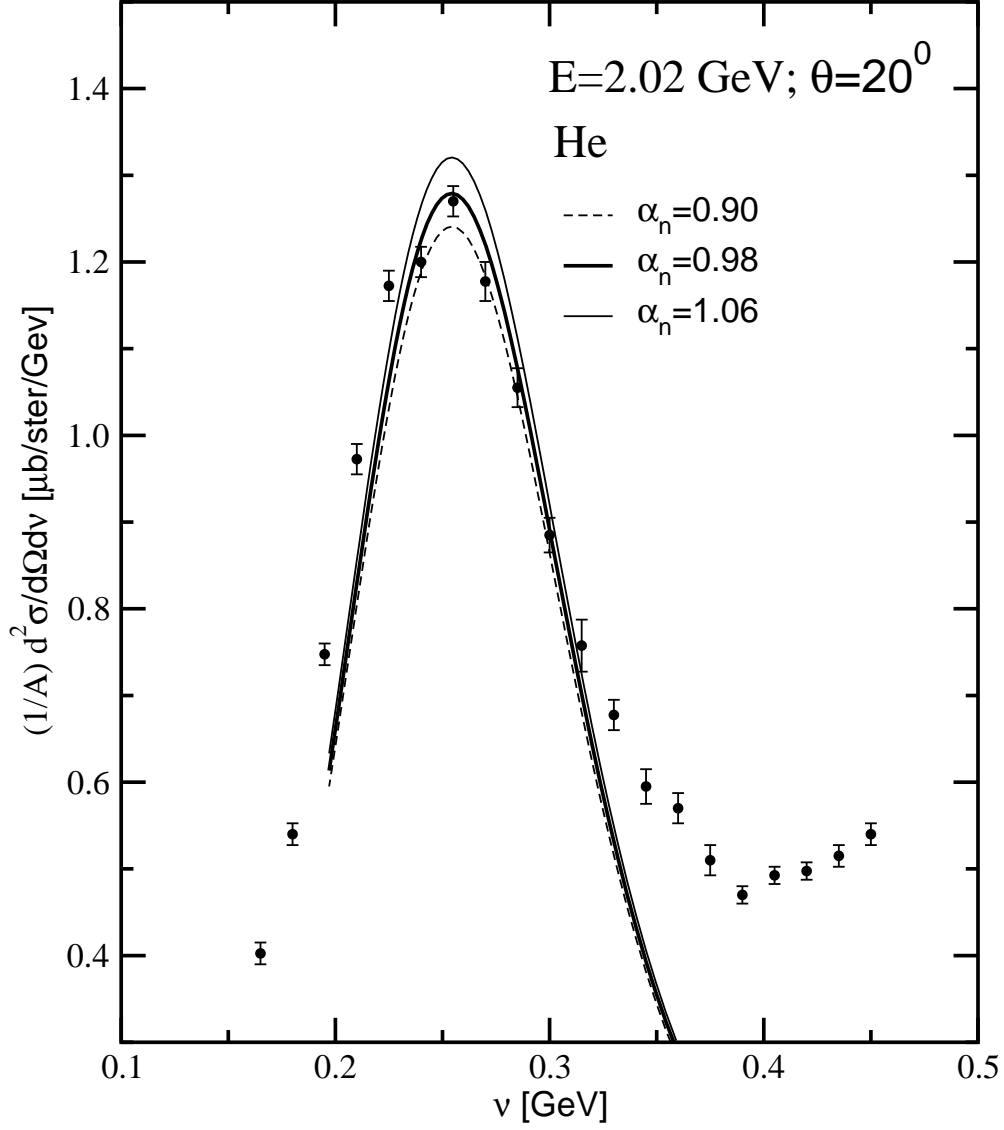


FIG. 6: Cross section for QE inclusive scattering of $E = 2.02 \text{ GeV}$ electrons on He for $\theta = 20^\circ$. Data are from Ref. [11]. The lines are the theoretical NE cross sections for three values of $\alpha_n(Q^2)$. The unbiased average value of $\alpha_n(Q^2)$ for this case can be found in Table II.

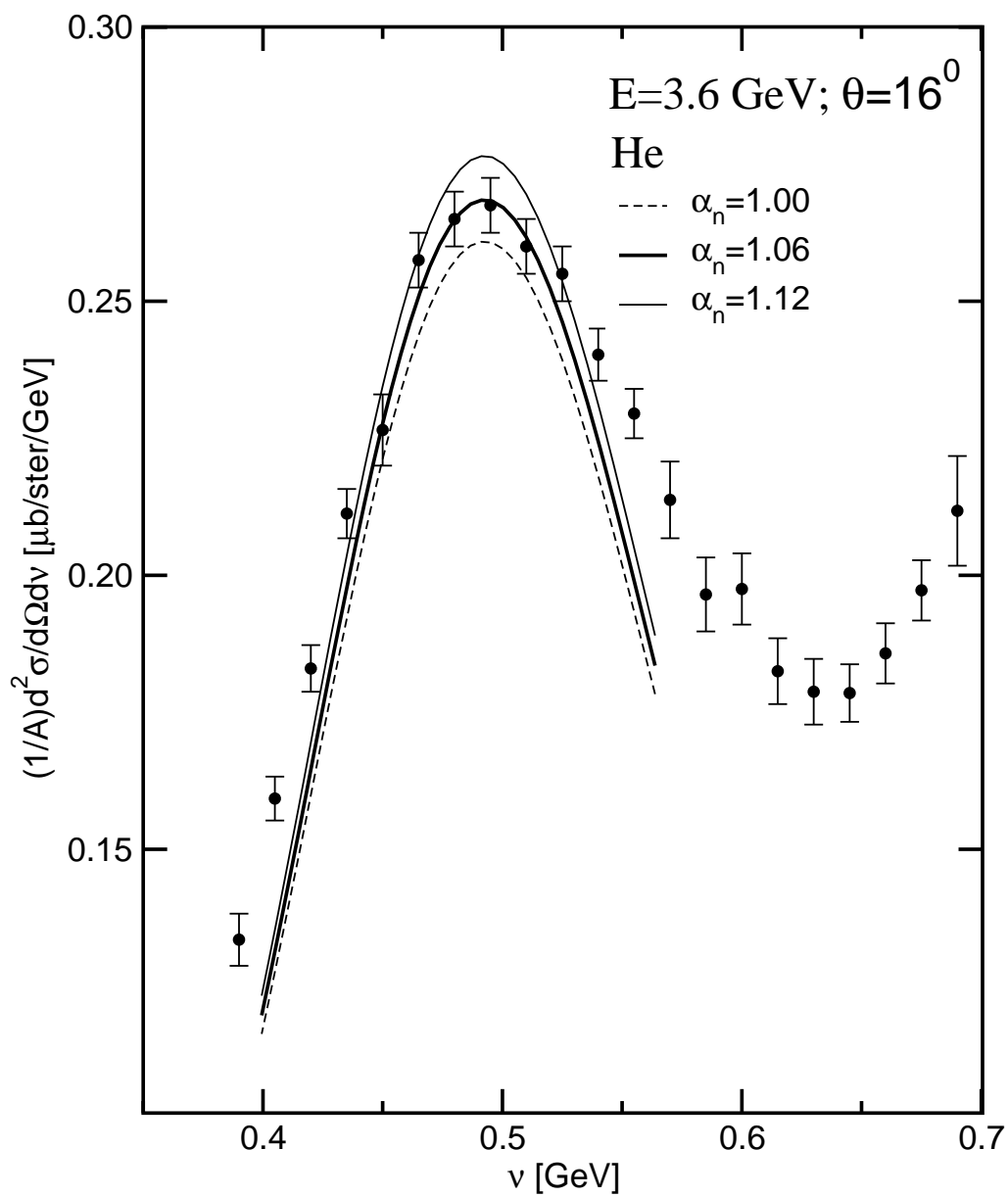


FIG. 7: The same as in Fig. 6 for $E=3.595 \text{ GeV}$, $\theta = 16^{\circ}$.

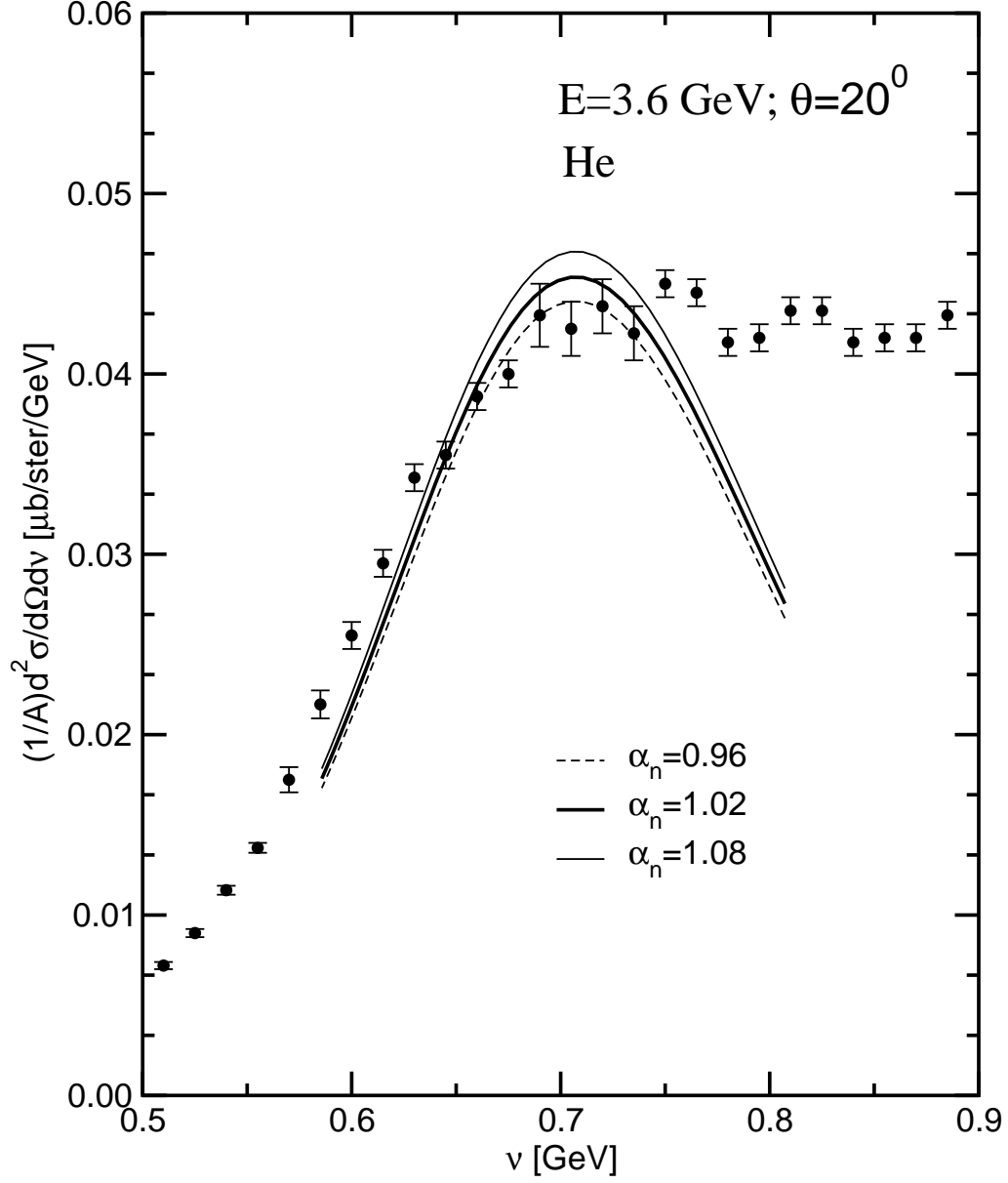


FIG. 8: The same as in Fig. 6 for $E=3.595 \text{ GeV}$, $\theta = 20^\circ$.

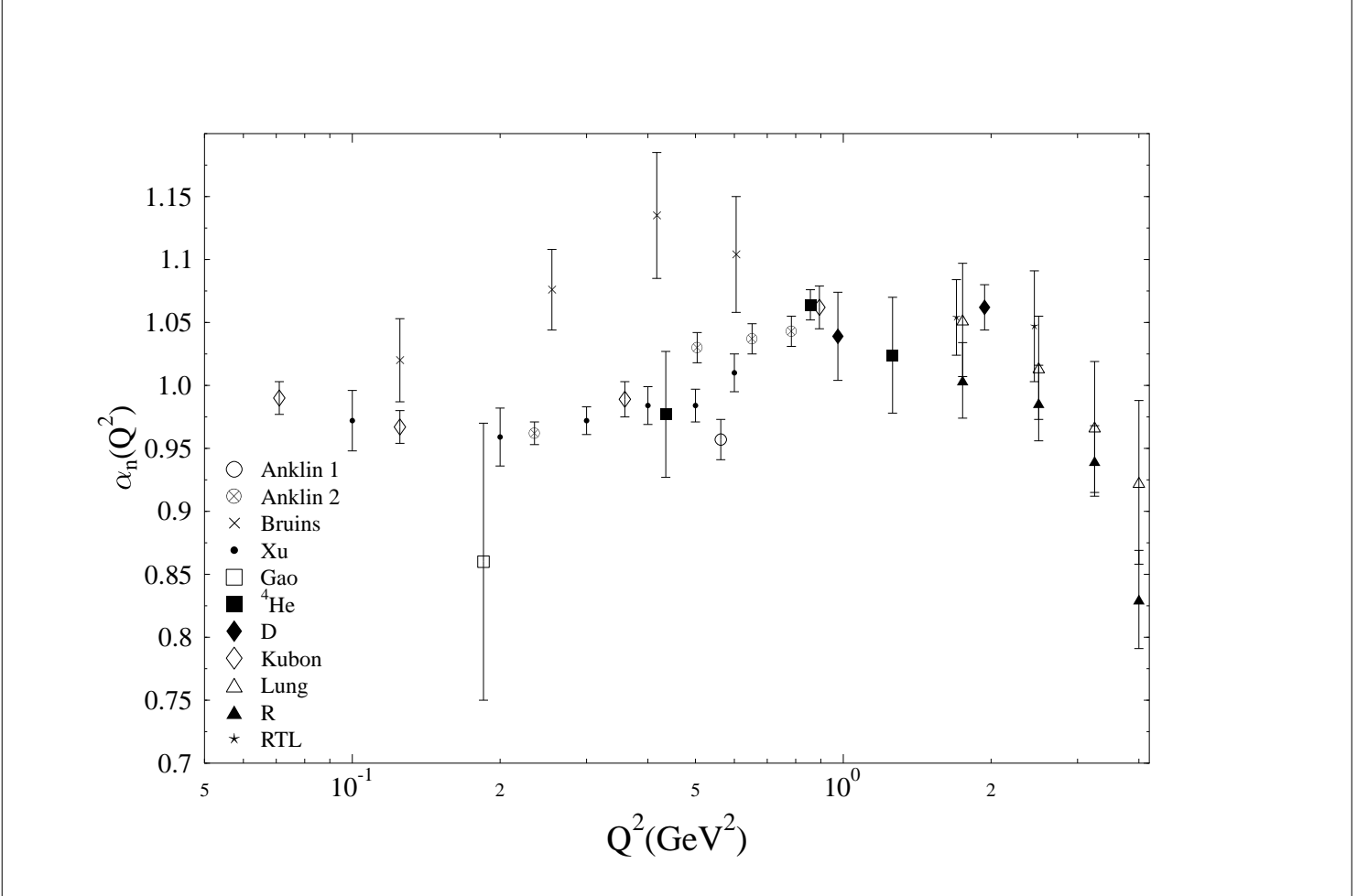


FIG. 9: $\alpha_n = G_M^n / \mu_n G_d$ as function of Q^2 . Entered are previous results and those obtained in the present work (filled squares, diamonds and triangles).

TABLE I: $N \rightarrow \Delta$ NI inclusive cross sections for D, ${}^4\text{He}$. Columns 1–4 give target, beam energy and scattering angle, $\langle Q^2 \rangle$ and x -position of the resonance for a number of values of the energy loss ν and x around the QEP. Moreover, in columns 5, 6 we report the NI cross sections computed with the $N \rightarrow \Delta$ excitation model described in Appendix B using $\Gamma_\Delta = 0.12$ GeV and $\Gamma_\Delta = 0$, respectively. In column 7, we report the NI cross section computed with Eq. (2.2) using the parametrized, resonance-averaged, nucleon SF $F_k^{N,NI}(x, Q^2)$. Finally, in the last column we report the measured (total) inclusive cross sections. All quantities are in powers of GeV; cross sections are in $\mu\text{b}/\text{ster}/\text{GeV}$

target	E, θ	$\langle Q^2 \rangle, x_\Delta$	ν, x	$\frac{1}{A} d^2 \sigma^{A, \Delta; \Gamma_\Delta}$	$\frac{1}{A} d^2 \sigma^{A, \Delta; \Gamma_\Delta=0}$	$\frac{1}{A} d^2 \sigma^{A, NI}$	$\frac{1}{A} d^2 \sigma_{\text{exp}}^{A, \text{total}}$
D [9, 10]	4.045, 15°	0.972, 0.601	0.465, 1.131	0.0193	0.0089	0.0162	0.178
			0.495, 1.054	0.0368	0.0130	0.0225	0.263
			0.525, 0.985	0.0656	0.0193	0.0627	0.435
			0.555, 0.922	0.0827	0.0295	0.1110	0.312
D [9, 10]	4.045, 23°	1.94, 0.750	0.975, 1.079	0.00195	0.00096	0.00050	0.0064
			1.005, 1.037	0.00325	0.00150	0.00084	0.0108
			1.035, 0.997	0.00531	0.00225	0.00138	0.0248
			1.065, 0.959	0.00806	0.00363	0.00232	0.0126
${}^4\text{He}$ [11]	2.02, 20°	0.434, 0.402	0.210, 1.125	0.0580	0.0202	0.256	0.973
			0.225, 1.035	0.0833	0.0281	0.386	1.173
			0.240, 0.962	0.1122	0.0382	0.535	1.200
			0.255, 0.898	0.1442	0.0504	0.704	1.270
${}^4\text{He}$ [11]	3.595, 16°	0.872, 0.575	0.420, 1.121	0.0322	0.0165	0.0297	0.183
			0.450, 1.037	0.0520	0.0259	0.0488	0.227
			0.465, 0.998	0.0629	0.0318	0.0607	0.258
			0.480, 0.963	0.0824	0.0399	0.0766	0.227
${}^4\text{He}$ [11]	3.595, 20°	1.266, 0.662	0.615, 1.119	0.008	0.0039	0.0029	0.0293
			0.645, 1.056	0.015	0.0086	0.0069	0.0343
			0.675, 0.999	0.021	0.0126	0.0105	0.0400
			0.705, 0.947	0.029	0.0186	0.0144	0.0425

TABLE II: Extraction of $\alpha_n(Q^2)$ from QE inclusive scattering data on D, ${}^4\text{He}$. Columns 1–4 give the target, the beam energy E , the scattering angle θ and the range of values of the Bjorken x variable chosen to perform the extraction of $\alpha_n(Q^2)$. Column 5 gives the corresponding range of values for Q^2 . Column 6 give the SF $f^{PN,A}(x, Q^2)$ for the extreme values of x in the range considered, and, in parenthesis, its maximal values reached when $x \approx 1$. The last column gives $\alpha_n(Q^2)$ with error of the mean over the considered x -range. The values between parenthesis are Lung's results without error bars.

target	E [GeV]	θ	x	Q^2 [GeV 2]	$f^{PN,A}(x, Q^2)$	$\alpha_n(Q^2)$
${}^4\text{He}$ [11]	2.02	20°	1.018-0.745	0.444-0.430	1.18-1.20 (1.49)	0.977±0.050
	3.595	16°	1.041-0.908	0.887-0.864	1.57-1.92 (1.92)	1.064±0.006
	3.595	20°	1.126-0.905	1.275-1.250	1.28-2.11 (2.16)	1.024±0.046
D [9, 10]	4.045	15°	1.131-0.953	0.988-0.972	1.31-3.65 (4.30)	1.039 ±0.035
	4.045	23°	1.079-0.978	1.976-1.929	2.44-5.18 (5.18)	1.062 ±0.018
D [3]	5.507	15.2°	1.063-0.978	1.769-1.741	2.89-5.04 (5.31)	1.055 ±0.047
	2.407	41.1°	1.081-0.957	1.803-1.721	2.37-4.89 (5.32)	1.050 ±0.017
	1.511	90.0°	1.059-0.977	1.812-1.728	3.21-4.79 (5.26)	1.057 ±0.023
$\mathcal{R}_T^{D,NE}$	3.809	20°	1.141-0.962	$\langle Q^2 \rangle = 1.75$	1.79-3.38 (5.31)	1.004±0.030 (1.052 ³)
D [3]	5.507	19.0°	1.104-1.000	2.561-2.501	1.69-5.65 (5.98)	1.032 ±0.035
	2.837	45.0°	1.101-0.991	2.613-2.500	1.69-5.91 (5.94)	1.031 ±0.043
	1.968	90.0°	1.064-0.984	2.608-2.474	3.06-5.71 (5.90)	1.078 ±0.055
$\mathcal{R}_T^{D,NE}$	5.016	20°	1.068-0.940	$\langle Q^2 \rangle = 2.50$	2.92-4.16 (5.94)	0.986±0.030 (1.014 ³)
$\mathcal{R}_T^{D,NE}$	5.016	20°	1.051-0.958	$\langle Q^2 \rangle = 3.25$	3.50-6.15 (6.43)	0.940±0.028 (0.967 ³)
$\mathcal{R}_T^{D,NE}$	5.016	20°	1.079-1.038	$\langle Q^2 \rangle = 4.00$	3.80-6.20 (6.50)	0.830±0.040 (0.923 ³)